Benefits of using a Wendland kernel for free-surface flows

F. Macià
A. Souto-Iglesias
Naval Architecture Dept.(ETSIN)
Technical University of Madrid (UPM)
28040 Madrid, Spain
fabricio.macia,antonio.souto@upm.es

M. Antuono
INSEAN
00128 Rome, Italy.
matteoantuono@gmail.com

A. Colagrossi
INSEAN
00128 Rome, Italy
CeSOS, NTNU,
Trondheim, Norway
a.colagrossi@insean.it

***Abstract*—The aim of this paper is to discuss the influence of the selection of the interpolation kernel in the accuracy of the modeling of the internal viscous dissipation in free surface flows. Simulations corresponding to a standing wave, for which an analytic solution is available, are presented. Wendland and renormalized Gaussian kernels are considered. The differences in the flow patterns and internal dissipation mechanisms are documented for a range of Reynolds numbers. It is shown that the simulations with Wendland kernels replicate the dissipation mechanisms more accurately than those with a renormalized Gaussian kernel. Although some explanations are hinted, we have failed to clarify which the core structural reasons for such differences are.**

Symbols

WC2	Wendland 5^{th} degree class 2 kernel
RGK	Renormalized Gaussian kernel

I. Introduction

In Colagrossi et al. [1], a theoretical analysis of the two most popular SPH formulations for Newtonian viscous terms, i.e. Monaghan's [2] and Morris *et al.*'s [3], was carried out at the continuous level. It was shown that in the presence of a free surface and under certain conditions, these viscous terms become singular with the inverse of the smoothing length. It was also demonstrated that for the Monaghan's [2] viscous term the singularity does not affect the integral flow quantities. As a consequence, the exact mechanical energy dissipation rate is recovered in the continuous approximation as the smoothing length goes to zero.

While in practical SPH implementations for pure diffusion processes, the viscous terms behave similarly [4], in order to assess the practical implications of the aforementioned results, a viscous free surface flow is simulated with SPH. Such flow is the evolution of a standing wave. This is a classical problem in the scientific literature and is of practical interest since it is strictly related to the propagation of gravity waves. Moreover, an analytic solution for the decay of the kinetic energy is available (see Lighthill [5]). The SPH simulations have been implemented using free-slip conditions along the solid boundary of the tank and using a renormalized Gaussian-Kernel [6]. and a fifth order class 2 Wendland [7] kernel. The aim of the present work is to document the benefits of using such a kernel when dealing with viscous free surface flows.

The paper is organized as follows: first, the physical problem we are interested in is presented. Second, the SPH model, emphasizing the properties of the considered kernels is introduced. Third, the practical problem considered, which has been the dissipation of the kinetic energy in a standing wave, is introduced and the results of the computations carried out, for a range of Reynolds numbers, are presented and discussed. Finally, some conclusions are drawn and future work threads hinted.

II. Governing equations

Free surface 2D laminar Newtonian incompressible flows are treated in this paper. The viscous effects in these flows are proportional to the Laplacian of the velocity field, $\boldsymbol{u}$. The equations that describe these flows are the Navier-Stokes incompressible ones.

In order to close this system of equations it is necessary to specify the boundary conditions (BC). Let the fluid domain be noted as Ω and its boundary as $\partial\Omega$. Such boundary encompasses a free surface boundary $\partial\Omega_F$ and solid boundaries $\partial\Omega_B$. Along the free surface, both a kinematic and a dynamic BC should be in principle fulfilled. They are not explicitly included in the SPH simulation, since the weakly compressible model is considered and such model can be properly shaped in order to being inherently consistent with the kinematic and pressure conditions [8] and simultaneously providing the correct viscous dissipation [1]. Notwithstanding that, the dynamic free surface BC is presented (equation 1 for the normal stress and 2 for the tangent stress) both for the sake of completeness and in order to recall that when viscosity is relevant, pressure is not in principle zero at the interface and is in general discontinuos.

$$p = 2\mu\, \boldsymbol{n} \cdot \partial \boldsymbol{u} / \partial \boldsymbol{n} \tag{1}$$

$$\boldsymbol{\tau} \cdot \mathbb{D} \cdot \boldsymbol{n} = 0 \tag{2}$$

In these equations $\boldsymbol{n}$ is the normal vector to the fluid domain, $\boldsymbol{\tau}$ is an unitary vector lying on the free surface tangent plane and $\mathbb{D}$ is the rate of strain tensor.

A free slip BC is imposed on the solid boundaries since we are interested in assessing the internal dissipation mechanisms and not those related to the solid boundaries.

III. SPH model

A. General

A weakly compressible approach is considered for the simulations [9]. The Monaghan's [2] viscous term is used, which, as mentioned in the introduction, allows in principle the computation of the exact mechanical energy dissipation rate since it is recovered in the continuous approximation as the smoothing length goes to zero.

B. Kernels

The kernels considered are the 5^{th} degree class 2 Wendland kernel [7], [10] and a renormalized Gaussian Kernel [4], [6]. They are both isotropic, which means that they can be written as:

$$W(\boldsymbol{x}, h) = \frac{1}{h^d}\tilde{W}(q) \tag{3}$$

where $\boldsymbol{x}$ is a vector in $\mathbb{R}^d$, h is the smoothing length, d is the dimensionality of the problem, and $q = |\boldsymbol{x}|/h$. They both have a compact support.

Wendland [7] devised a family of radial interpolation functions that have compact support and that are definite positive. We have used the 5^{th} degree class 2 Wendland kernel (WC2 from now on) reformulating it so that it has a $2h$ radius support, similarly to Robinson et al. [10], [11].

$$\tilde{W}_{WC2}(q) = \beta \begin{cases} (2-q)^4(1+2q) & \text{for } 0 \le q \le 2 \\ 0 & \text{for } q > 2 \end{cases} \tag{4}$$

where d is the dimensionality of the kernel and β is a constant that depends on d and that is equal to $7/(64\pi)$ in 2D, which is how the simulations have been carried out.

Together with the Wendland kernel, the renormalized Gaussian kernel (RGK from now on) of Molteni and Colagrossi [6] has bee also considered. According to [6], from a numerical point of view the behavior of the RGK is almost identical to the classical Gaussian kernel and the following properties are well established: (i) amongst 10 tested kernel shapes, the Gaussian kernel appears to give the best numerical accuracy in the stable field [12]; (ii) the comparison of the Gaussian kernel to classically used spline kernels showed that the former leads to better stability properties [13]; (iii) it presents also a lower computational cost with respect to evolved forms of spline kernels [14]; finally, (iv) its gradient can be straightforwardly obtained from the evaluation of the kernel itself.

Since the radius of Molteni and Colagrossi RGK [6] is $3h$, we have reformulated it (equation 5) so that its radius is $2h$ and thus be possible to compare its performance with the Wendland kernel one, using the same parameters:

$$\tilde{W}_{RGK}(q) = M_\alpha \begin{cases} \exp(-\alpha^2\, q^2) - m_\alpha & \text{for } 0 \le q \le 2 \\ 0 & \text{for } q > 2 \end{cases} \tag{5}$$

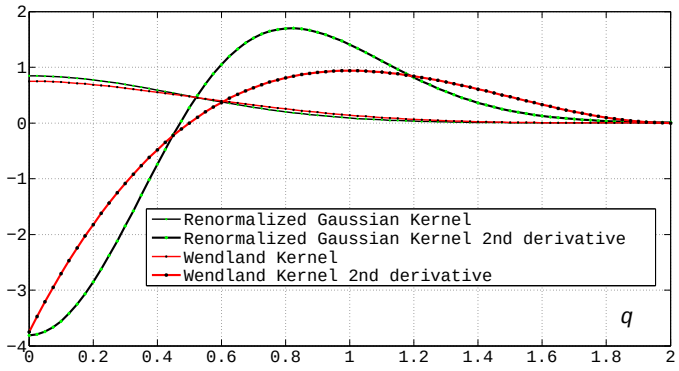

Fig. 1. Wendland and Gaussian Kernels

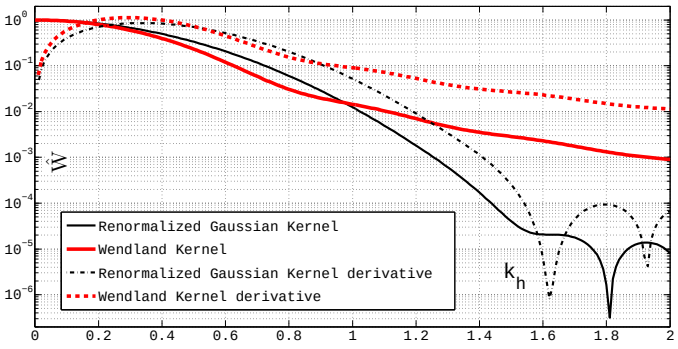

Fig. 2. Fourier transforms. The normalized wave number k_h is scaled so that $k_h = 1$ for the mode with wavelength $\lambda = h$

Where $\alpha = 3/2$, and in 2D $M_{3/2} = 0.717082$ and $m_{3/2} = \exp(-9)$. A plot of both kernels and their second derivatives is presented in figure 1.

Tensile instability may arise, according to [15], when a particle enters in the negative second derivative region of the neighborhood of another particle and the pressure is positive. As can be appreciated in figure 1, the size of these regions is very similar for both kernels ($q < 0.5$ for $\tilde{W}_{WC2}$ and $q < \sqrt{2}/3 \sim 0.4714$ for $\tilde{W}_{RGK}$), which suggests they should behave similarly in regards to the onset of such instability. We will see this is not the case. Morris [13] showed that the Fourier transform of the kernels is relevant for the stability of SPH simulations. He found that stability is improved if the transforms fall off rapidly. If we look at the spectrum of both kernels (figure 2), we find that the RGK spectral components are smaller than WC2's for wave numbers greater than the corresponding to h. This would suggest that the RGK should filter the high frequency oscillations better than the WC2. We will see that this is not the case. Robinson [11] got to a similar conclusion, when comparing WC2 to spline kernels.

IV. Results

A. General

Simulations corresponding to the dissipation of kinetic energy in a viscous standing wave have been conducted. There

is an analytic solution by Lighthill [5] to compare to that is also presented. A range of Reynolds numbers, resolutions and number of neighbors has been covered in the simulations. The results are documented in this section, showing the diverse performance of the RGK and WC2 kernels.

B. Dissipative effects for Standing Waves

In the following, H denotes the still water depth, L is the tank length, λ the wave length of the standing wave (which will be taken as L in our simulations) and k the corresponding wave number (*i.e.* $k = 2\pi/\lambda$). The standing wave amplitude is indicated by A while ϵ denotes the ratio $2A/H$. For small-amplitude waves (*i.e* small ϵ), and small wave steepness (*i.e* $2A/\lambda \ll 0.1$) the potential theory gives the following approximate analytical solution (see figure IV-B for a sketch of the flow domain and initial velocity vectors)):

$$\varphi(x,y,t) = \varphi_0(x,y)\,\cos(\omega\,t) \tag{6}$$

$$\varphi_0(x,y) = -\,\epsilon\,\frac{H\,g}{2\,\omega}\,\frac{\cosh[k(y+H)]}{\cosh(kH)}\,\cos(k\,x) \tag{7}$$

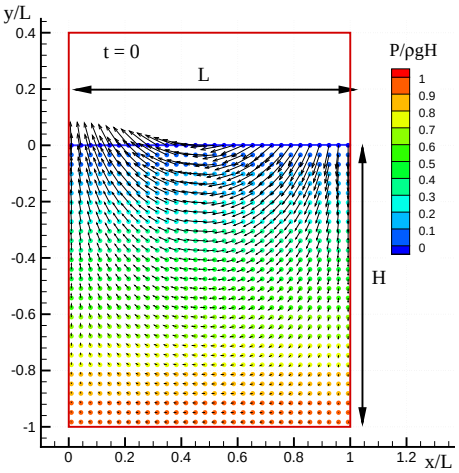

Fig. 3. Sketch of the standing wave problem and initial velocity field

The period of oscillation of the standing waves is $T = 2\pi/\omega$ where the circular frequency ω is given by the dispersion relation: $\omega^2 = g\,k\,\tanh(k\,H)$ and g is the gravity acceleration. We set the time origin $t = 0$ when the free surface is horizontal and the time derivative of the velocity potential $\dot{\varphi}$ is zero in the whole domain. In this way, the pressure field can be simply assumed to be hydrostatic with an error of $O(\epsilon^2)$. By definition the initial fluid velocity is given by $\nabla\varphi_0$. For an inviscid fluid, the linear theory predicts that the standing wave evolves infinitely without any change of amplitude, i.e. the total energy is conserved. For viscous fluid an analytical approximation of the kinetic energy dissipation can be derived following the procedure described by Lighthill [5]. This reads:

$$E_{kin}(t) \;=\; \epsilon^2\,g\,\frac{\lambda\,H^2}{32}\,e^{-4\,\nu\,k^2\,t}\,[\,1\;+\;\cos(2\,\omega\,t)\,] \tag{8}$$

where ν is the kinematic viscosity of the fluid. The damping coefficient is $\beta = 4\,\nu\,k^2$ and depends on the wave number and on the kinematic viscosity. Lighthill [5] obtained this result by substituting the linear solution (6) into the dissipative term of the kinetic energy, that is:

$$\mathscr{D} \;=\; \int (\mathbb{D} : \mathbb{D})\,dV \;=\; \int (\,\varphi_{xx}^2 \;+\; 2\,\varphi_{xy}^2 \;+\; \varphi_{yy}^2\,)\,dV\,, \tag{9}$$

and, then, averaging over a wave period. In this context we are neglecting the influence of solid boundaries and of the bottom friction.

In the work of Wu et al. [16], the linearized Navier-Stokes equations are solved to inspect the influence of viscosity on free-surface waves evolving into a two-dimensional tank. To justify the use of the linearized equations, Wu et al. [16] assumed $\epsilon \ll 1$ similarly to what was done to get the solution (6). Further, they imposed a free-slip condition along the solid boundaries. Under these hypotheses, the evolution of the potential energy for the standing wave is:

$$\frac{E_p(t)}{E_p(0)} = \left\{ \frac{16\,\pi^6}{Re^4} + \frac{8\,\pi^3}{Re^2}\,e^{-\alpha\,t}\left[\cos\!\left(\sqrt{gk}\,t\right) + \frac{2\,\pi^{3/2}}{Re}\,\sin\!\left(\sqrt{gk}\,t\right)\right] + e^{-2\,\alpha\,t}\left[\cos\!\left(\sqrt{gk}\,t\right) + \frac{2\,\pi^{3/2}}{Re}\,\sin\!\left(\sqrt{gk}\,t\right)\right]^2 \right\} \Big/ \left(1 + \frac{4\,\pi^3}{Re^2}\right)^2 \tag{10}$$

where $Re = H\,\sqrt{gH}/\nu$ is the Reynolds number and $\alpha = 2\,\nu\,k^2$. Under the hypotheses:

$$1 \;\ll\; Re \qquad \text{and} \qquad \sqrt{gk}\,t \;\ll\; \frac{Re}{2\,(kH)^{3/2}}\,\log\!\left(\frac{Re^2}{8\,\pi^3}\right), \tag{11}$$

the potential energy in (10) behaves as:

$$E_p(t)/E_p(0) \;\simeq\; e^{-2\,\alpha\,t}\,\cos\!\left(\sqrt{gk}\,t\right). \tag{12}$$

This expression shows that, for short times, the damping rate of gravity waves is $\beta = 2\,\alpha = 4\,\nu\,k^2$. Such a damping coefficient coincides with that found by Lighthill [5].

C. Simulations setup

The initial arrangement of the particles is a cartesian lattice (figure 4). Tentative computations with other arrangements suggest that the conclusions do not depend on the arrangement type. Ghost particles (see e.g. [9]) are used to enforce the free slip boundary condition. Simulations have been carried out for both kernels covering a range of Reynolds numbers, resolutions and in some particular cases different dx/h ratios. A summary of the simulations parameters is presented in table I. The trends observed for $Re = 500$ are maintained for $Re = 1000, 2000$ and relevant changes appear for $Re = 5000$. Therefore, due to lack of space, the results for the intermediate Reynolds number cases are skipped in the present paper. The simulations have been conducted assuming the regime is laminar. This assumption is valid for the range of Reynolds numbers considered, as shown in reference [17], where transitional flows were described for $Re > 20000$. Moreover, free slip boundary conditions have been used, which prevent the generation of vorticity close to the walls. In order

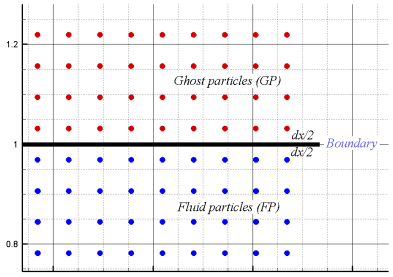

Fig. 4. Initial condition lattice of the particles. dx is the typical particle spacing.

TABLE I
CHARACTERISTICS OF THE SIMULATIONS

Re	Kernel	H/dx	dx/h
500	WC2, RGK	50, 100, 200, 400	0.5
	WC2	200	1/3
	RGK	200	2/9
1000	WC2, RGK	100, 200, 400	0.5
2000	WC2, RGK	100, 200, 400	0.5
5000	WC2, RGK	100, 200, 400,800	0.5
	WC2	400	1/3, 1
	WC2	100, 200, 400, 800	0.2
	RGK	400	1/3, 2/3, 2/9

to check that the decay rates presented in section IV-B are valid for Reynolds numbers of the same order of the ones that will be used in our computations, simulations with a well established VOF solver, STAR-CCM+ [18], have been conducted.

In regards to specific details of the SPH implementation for this problem (initial condition for the pressure, free slip boundary conditions, etc.) we refer to reference [19].

D. Results for Re = 500

Results for the decay of the Kinetic Energy as predicted by using the Monaghan's [2] viscosity formula and Lighthill's [5] reference solution (dashed black line) are presented for RGK and WC2 kernels in figure 5. The curves correspond to the highest resolution H/dx = 400 and to dx/h = 0.5, which means that each particle has around 50 neighbors. As can be appreciated, the agreement with the exact solution is good, though SPH tends to underestimate the decay rate, which is more evident for the WC2 simulation.

The vorticity field is now analyzed. Vorticity is computed by differentiating the velocity field using MLS correction for the SPH interpolation [20]. Results are presented for one instant of the first oscillation cycle in figure 6. This figure shows the onset of the viscous boundary layer at the free-surface due to the unbalance of the zero stress boundary condition. Both kernels perform yet similarly at this stage.

If the simulation is run for a few more periods, the differences between both kernels results can be clearly appreciated, as the vorticity field of the RGK one becomes noisy (figure 7). This means that a certain amount of kinetic energy is being lost in these numerical fluctuations, which

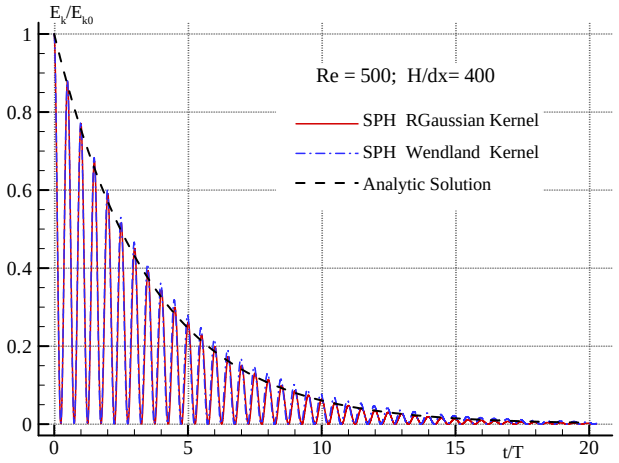

Fig. 5. Kinetic energy decay, dx/h = 0.5, Re = 500, H/dx = 400

could explain the gap in the kinetic energy decay rate curves observed in figure 5. This dissipation of energy through numerical fluctuations was analyzed in other context by Ellero et al [21], by showing the analogy with the dissipation mechanism at molecular level.

Observing figure 7(b) it seems that the instabilities are somehow related to the effect of the bottom boundary but that is not clear yet at this stage. In addition, the structure of the RGK kernel vorticity field suggests that tensile instability may have been excited while that is not the case for the WC2 kernel. This is unexpected since the pressure field is a compression one due to the effect of the hydrostatic pressure and for dx/h = 0.5 particles are not into the negative second derivative region of the kernel. Robinson [11] showed in forced turbulence simulations that the WC2 kernel prevented the clustering of particles, keeping them at relative distances close to the initial lattice. In our particular case, the initial distribution of the particles can be described by figure 8 where $\mathcal{H}$ is a histogram of particle pairs distances for particles inside the support of the kernel and R_ρ is the radial particle density function, as defined by Robinson [11]. This function is a good indicator of particle clustering. It is plotted for both kernels in a later cycle in figure 9 and the differences can be clearly appreciated; the WC2 kernel keeps the relative distance between particles whilst the RGK ones present a significant scatter but not a clustering of neighboring particles. This scatter induces extra inaccuracies in the evaluation of the SPH operators, as discussed by [22], [23] but its origin and link with the structure of the kernels is not clear at this stage.

In order to check whether the instability is being excited for the RGK, the ratio dx/h was made smaller (from 0.5 to 2/9=0.222, which means passing from 50 to 250 neighbors) so that at least there are two rings of neighbors inside the negative kernel second derivative region, whose bounds have been shown in section III-B. On one side, the noise in the vorticity field is significantly reduced, the kinetic energy increases with respect to the resolution dx/h = 0.5 (less spurious dissipation)

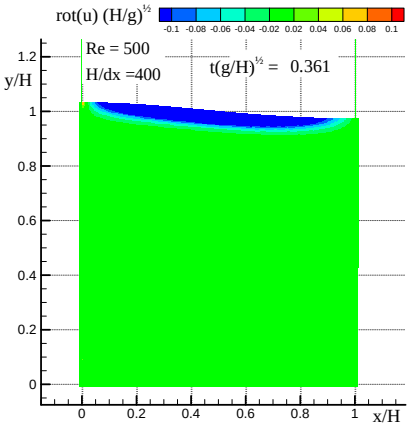

(a) WC2

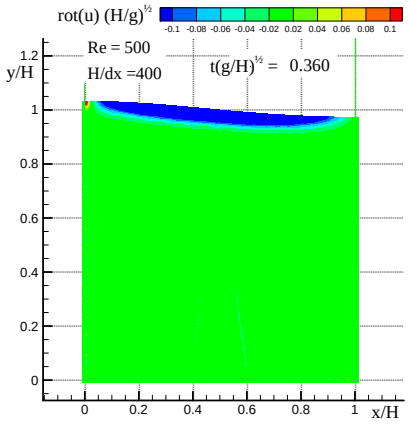

(b) RGK

Fig. 6. Vorticity, $Re = 500$, $dx/h = 0.5$, $t(g/H)^{0.5} = 0.361$, $H/dx = 400$

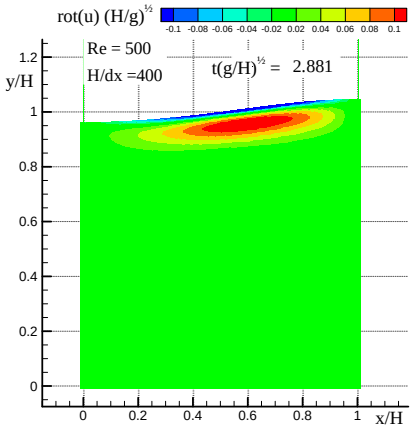

(a) WC2

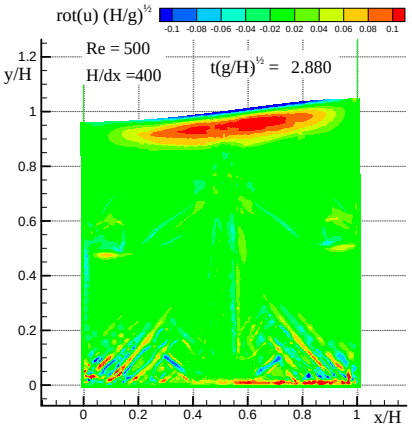

(b) RGK

Fig. 7. Vorticity, $Re = 500$, $dx/h = 0.5$, $t(g/H)^{0.5} = 2.880$, $H/dx = 400$.

and gets closer to the one provided by WC2 kernel for that resolution (figure 10), which presents less dissipation than the exact solution. In regards to the radial particle density function, it shows scattering from the initial configuration (figure 11). in a similar manner as in the case with $dx/h = 0.5$. We would expect to have less scattering due to the vorticity field being smoother but it seems this is not the case. Also we would expect the triggering of the tensile instability because there are particles with positive pressure in an area of negative second derivative of the kernel, but it seems no clustering of neighbors is taking place.

E. Results for Re = 5000

The kinetic energy evolution is shown in figure 12. It is noticeable that due to the reduction in viscosity there is still 60% of the kinetic energy after 20 oscillations, compared to less than 1% for the $Re = 500$ case (figure 5). As the Reynolds number gets higher, the gradients of vorticity in the region close to the free surface become larger; therefore it becomes more difficult to resolve them. This is reflected in the boundary layers being thinner (figure 13) than the ones shown in figure 6, corresponding to $Re = 500$.

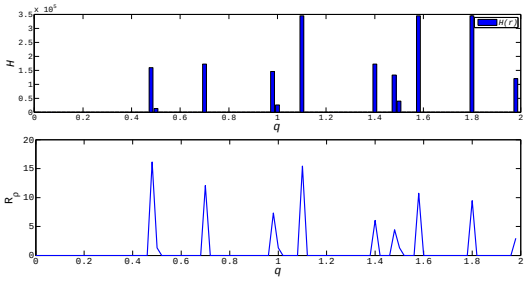

Fig. 8. Particle density graph for $t(g/H)^{0.5} = 0$, $H/dx = 400$.

The simulations with the WC2 kernel are now more dissipative than the exact solution. This could be due to the spurious vorticity that is created mainly in the lateral walls, for which we have found yet no explanation (figure 14(a)). The noise in the RGK simulations is now even more intense and the scales of the noise are spread through a wide range (figure 14(b)) including elongated structures; the reason for these patterns is left for future studies. Since we are finding some inaccuracies in the WC2 simulations, it makes sense to observe the radial particle density graphs for a late frame of

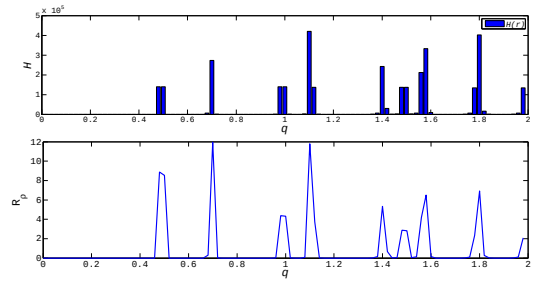

(a) WC2

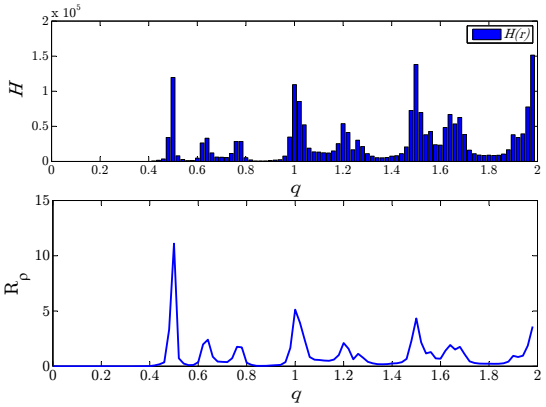

(b) RGK

Fig. 9. Particle density, $Re = 500$, $dx/h = 0.5$, $t(g/H)^{0.5} = 17.641$, $H/dx = 400$.

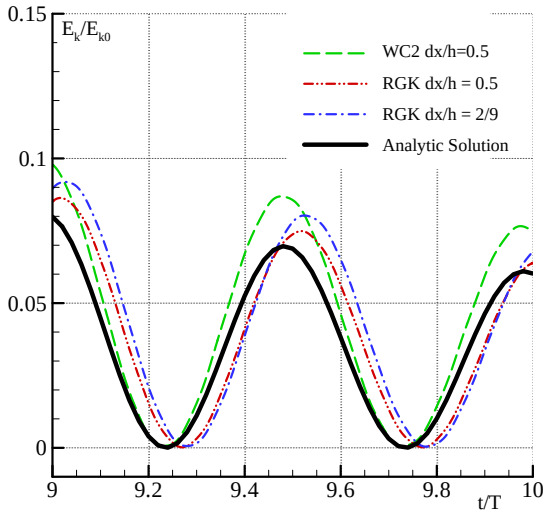

Fig. 10. Kinetic energy, RGK, $dx/h = 0.5, 2/9$, $Re = 500$, $H/dx = 200$

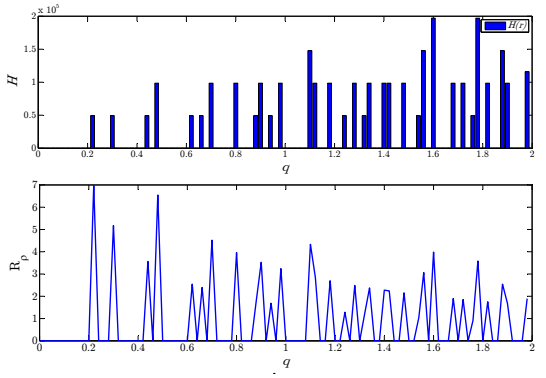

(a) $t(g/H)^{0.5} = 0$

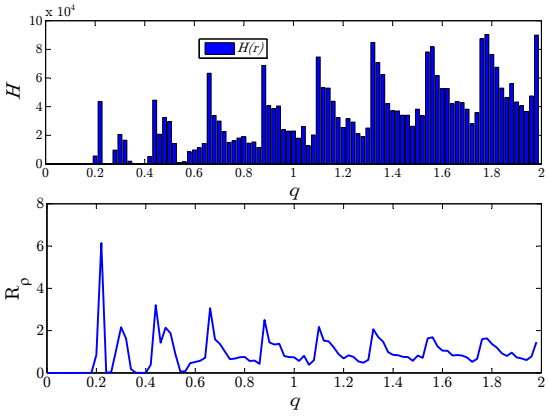

(b) $t(g/H)^{0.5} = 17.641$

Fig. 11. Particle density graph for RGK, $dx/h = 2/9$, $H/dx = 200$.

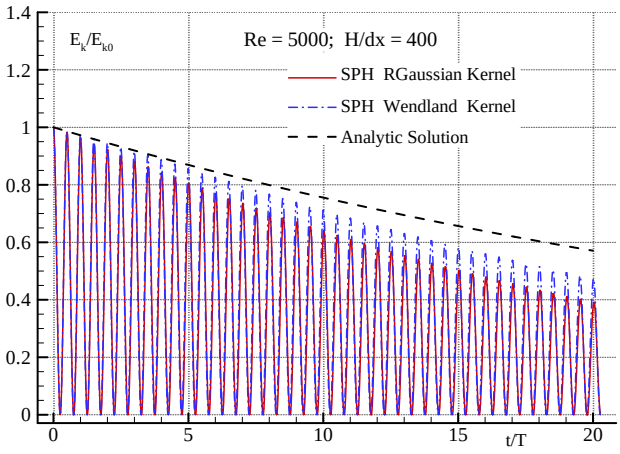

Fig. 12. Kinetic energy decay, $dx/h = 0.5$, $Re = 5000$, $H/dx = 400$

these simulations. This is done in figure 15, where it can be appreciated that the dispersion in the particles position for the WC2 is yet small, while large, as expected, for the RGK one.

If we decrease the ratio dx/h in order to get closer to the continuum, the noise in the simulations with the WC2 kernel disappear and the decay rate tends to the exact one (figure 16). With the RGK the particles cluster in some regions of the flow domain (figure 17), in a similar pattern like the one corresponding to the tensile instability phenomenon. If we take a look at the radial particle density function (figure 17) we see that the clustering is reflected in the density reaching its peak for $q = 0$. This clustering does not take place under the same conditions for the WC2 simulations.

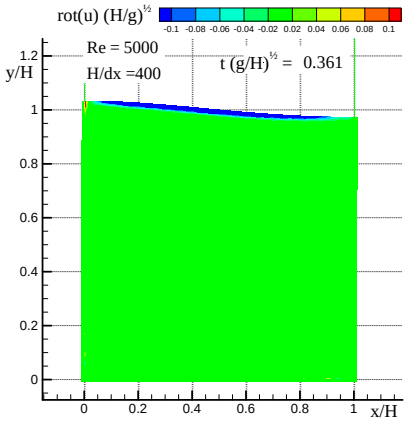

Fig. 13. Vorticity, $Re = 5000$, WC2, $dx/h = 0.5$, $t(g/H)^{0.5} = 0.361$, $H/dx = 400$

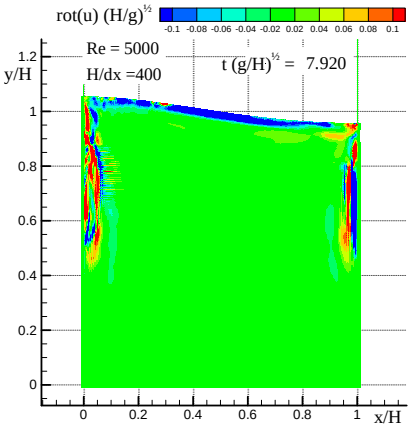

(a) WC2

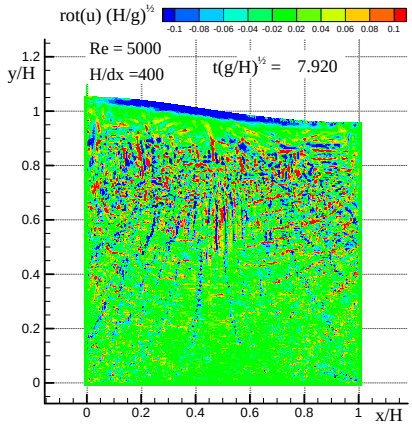

(b) RGK

Fig. 14. Vorticity, $Re = 5000$, $dx/h = 0.5$, $t(g/H)^{0.5} = 7.920$, $H/dx = 400$.

V. Conclusions and future work

The aim of this paper has been to discuss the performance of two significant kernels in simulating free surface viscous flows. The kernels considered have been the 5th degree class 2 Wendland kernel and a renormalized Gaussian Kernel. The

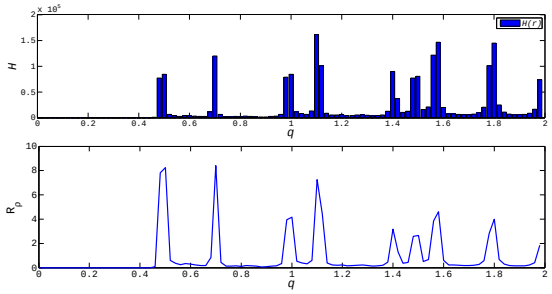

(a) WC2

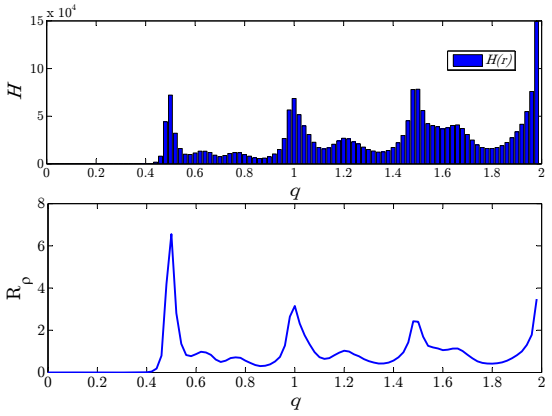

(b) RGK

Fig. 15. Particle density, $Re = 5000$, $t(g/H)^{0.5} = 17.641$, $dx/h = 0.5$, $H/dx = 400$.

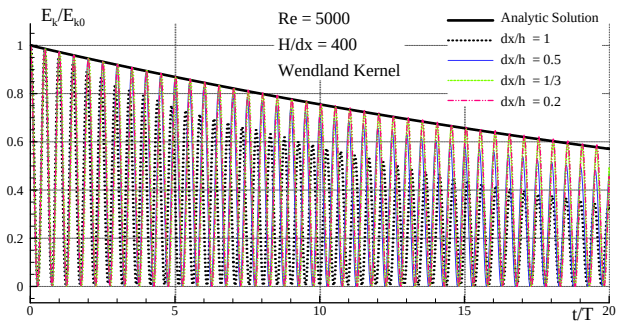

Fig. 16. Kinetic energy decay, WC2, $Re = 5000$, $H/dx = 400$

evolution of a standing wave has been simulated using both kernels. It is a significant test case because a analytical solution for the kinetic energy decay rate is available. Simulations have been conducted varying the Reynolds number, resolution and number of neighbors. It has been found that Wendland kernel simulations provide better results. For the low Reynolds number cases, the renormalized Gaussian kernel simulations show a noisy vorticity field but no clustering takes place. For the highest Reynolds number case and for the largest neighbors number, the renormalized Gaussian kernel simulations present a clustering of neighbors due to the onset of the tensile instability, which in the same conditions, does not take place for the Wendland kernel simulations. We have not been

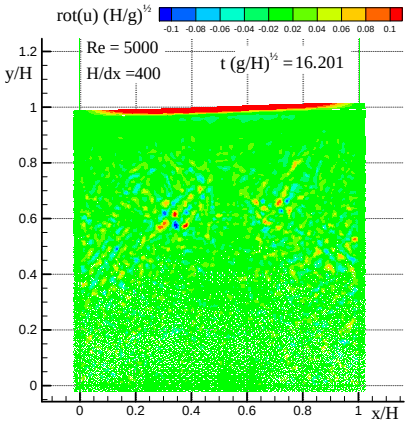

(a)

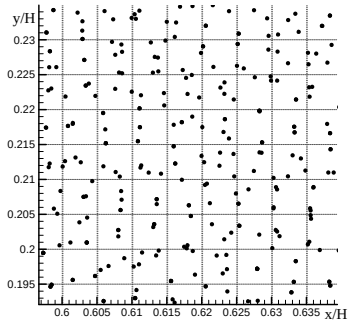

(b) zoom

Fig. 17. Vorticity, Re = 5000, dx/h = 2/9, $t(g/H)^{0.5}$ = 16.201, H/dx = 400.

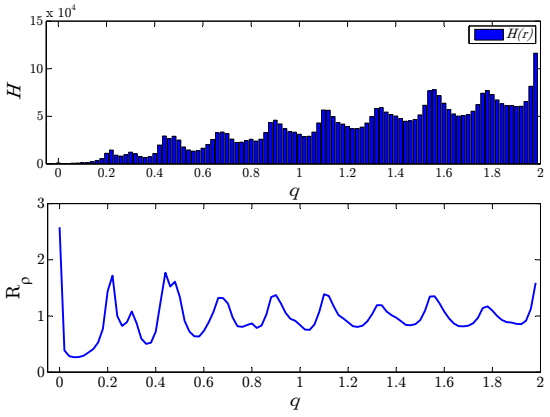

Fig. 18. Particle density, Re = 5000, $t(g/H)^{0.5}$ = 16.201, dx/h = 2/9, H/dx = 400.

able to link the discrepancies found with the properties of both kernels. Nonetheless, we think that Wendland kernel provides better results and should therefore be used on top of Renormalized Gaussian for free surface flows simulations.

Acknowledgments

The research that backs this paper has received funding from the European Community's FP7 under grant agreement n225967 "NextMuSE", from the Centre for Ships and Ocean Structures (CeSOS), NTNU, Trondheim, within the "Violent Water-Vessel Interactions and Related Structural Load" project and from the Spanish Ministry for Science and Innovation under grant TRA2010-16988 "Caracterización Numérica y Experimental de las Cargas Fluido-Dinámicas en el transporte de Gas Licuado"

References

[1] A. Colagrossi, M. Antuono, A. Souto-Iglesias, D. Le Touzé, and P. Izaguirre-Alza, "Theoretical analysis of SPH in simulating free-surface viscous flows," in *5th ERCOFTAC SPHERIC workshop*, 2010.

[2] J. J. Monaghan and R. A. Gingold, "Shock simulation by the particle method SPH," *J. Comp. Phys.*, vol. 52, no. 2, pp. 374–389, 1983.

[3] J. P. Morris, P. J. Fox, and Y. Zhu, "Modeling low Reynolds number incompressible flows using SPH," *J. Comp. Phys.*, vol. 136, 1997.

[4] F. Macià, J. M. Sánchez, A. Souto-Iglesias, and L. M. González, "WCSPH viscosity diffusion processes in vortex flows," *International Journal for Numerical Methods in Fluids*, (in press).

[5] J. Lighthill, *Waves in fluids*. Cambridge University Press, 2001.

[6] D. Molteni and A. Colagrossi, "A simple procedure to improve the pressure evaluation in hydrodynamic context using the SPH," *Computer Physics Communications*, vol. 180, pp. 861–872, 2009.

[7] H. Wendland, "Piecewise polynomial, positive definite and compactly supported radial functions of minimal degree," *Adv. Comput. Math.*, vol. 4, no. 4, pp. 389–396, 1995.

[8] A. Colagrossi, M. Antuono, and D. L. Touzé, "Theoretical considerations on the free-surface role in the Smoothed-particle-hydrodynamics model," *Physical Review E*, vol. 79, no. 5, 2009.

[9] A. Colagrossi and M. Landrini, "Numerical simulation of interfacial flows by smoothed particle hydrodynamics," *J. Comp. Phys.*, vol. 191, pp. 448–475, 2003.

[10] M. Robinson and J. Monaghan, "Forced 2D wall-bounded turbulence using SPH," in *3rd SPHERIC workshop*, 2008, pp. 78–84.

[11] M. Robinson, "Turbulence and Viscous Mixing using Smoothed Particle Hydrodynamics," Ph.D. dissertation, Department of Mathematical Science, Monash University, 2009.

[12] J. Hongbin and D. Xin, "On criterions for smoothed particle hydrodynamics kernels in stable field," *Journal of Computational Physics*, vol. 202, no. 2, pp. 699 – 709, 2005.

[13] J. Morris, "Analysis of SPH with applications," Ph.D. dissertation, Mathematics Dpt., Monash Univ., Melbourne, Australia, 1996.

[14] A. Colagrossi, "A meshless lagrangian method for free-surface and interface flows with fragmentation," Ph.D. dissertation, Università di Roma La Sapienza, 2005.

[15] J. W. Swegle, D. L. Hicks, and S. W. Attaway, "Smoothed Particle Hydrodynamics Stability Analysis," *Journal of Computational Physics*, vol. 116, pp. 123–134, 1995.

[16] G. X. Wu, R. Eatock-Taylor, and D. M. Greaves, "The effect of viscosity on the transient free-surface waves in a two-dimensional tank," *J. Engng. Maths.*, vol. 40, pp. 77–90, 2001.

[17] A. Cenedese, "Transition from Laminar to Turbulent Flow inside an Oscillating Tank," *Meccanica*, vol. 18, pp. 217–224, 1983.

[18] I. Demirdzic and S. Muzaferija, "Numerical method for coupled fluid flow, heat transfer and stress analysis using unstructured moving meshes with cells of arbitrary topology," *Computer Methods in Applied Mechanics and Engineering*, vol. 125, no. 1-4, pp. 235 – 255, 1995.

[19] M. Antuono, A. Colagrossi, S. Marrone, and C. Lugni, "Propagation of gravity waves through an SPH scheme with numerical diffusive terms," *Computer Physics Comm.*, vol. 182, no. 4, pp. 866 – 877, 2011.

[20] A. Colagrossi, G. Colicchio, C. Lugni, and M. Brocchini, "A study of violent sloshing wave impacts using an improved SPH method," *Journal of Hydraulic Research*, vol. 48, no. Extra Issue, pp. 94–104, 2010.

[21] M. Ellero, P. Español, and N. A. Adams, "Implicit atomistic viscosities in smoothed particle hydrodynamics," *Phys. Rev. E*, vol. 82, no. 4, 2010.

[22] N. J. Quinlan, M. Lastiwka, and M. Basa, "Truncation error in mesh-free particle methods," *International Journal for Numerical Methods in Engineering*, vol. 66, no. 13, pp. 2064–2085, 2006.

[23] A. Amicarelli, J.-C. Marongiu, F. Leboeuf, J. Leduc, and J. Caro, "SPH truncation error in estimating a 3D function," *Computers & Fluids*, vol. 44, no. 1, pp. 279 – 296, 2011.